1 **Small-angle neutron scattering reveals the effect of Mo on interphase nano-precipitation**

2 **in Ti-Mo micro-alloyed steels**

3

4 Y. Q. Wang[a*, b], S. J. Clark[b, c], B. Cai[d], D. Alba Venero[e], K. Yun[f], M. Gorley[a], E. Surrey[a], D.

5 G. McCartney [b, g], S. Sridhar[h], P. D. Lee[b, c*]

6

7 [a] *United Kingdom Atomic Energy Authority, Culham Science Centre, Abingdon, OX14 3DB, UK*

8 [b] *Research Complex at Harwell, Rutherford Appleton Laboratory, Harwell, OX11 0FA, Oxfordshire, UK*

9 [c] *Department of Mechanical Engineering, University College London, Torrington Place, London WC1E 7JE, UK*

10 [d] *School of Metallurgy and Materials, University of Birmingham, Birmingham, UK*

11 [e] *ISIS, STFC Rutherford Appleton Laboratory, Didcot, Oxfordshire, OX11 0QX, UK*

12 [f] *School of Materials, University of Manchester, Manchester, M13 9PL, UK*

13 [g] *Advanced Materials Group, University of Nottingham, Nottingham, NG7 2RD, UK*

14 [h] *George S. Ansell Department of Metallurgical and Materials Engineering, Colorado School of Mines, Golden,*

15 *CO 80401, USA*

16 [*] Corresponding authors: Yiqiang Wang (yiqiang.wang@ukaea.uk) and Peter Lee (peter.lee@ucl.ac.uk)

17

18

19

20

21

1 **Abstract**

2 Ti-containing micro-alloyed steels are often alloyed with molybdenum (Mo) to reduce nano-

3 precipitate coarsening, although the mechanism is still disputed. Using small angle neutron

4 scattering we characterised the precipitate composition and coarsening of Ti-alloyed and Ti-

5 Mo-alloyed steels. The results demonstrate ~25 at.% of Ti is substituted by Mo in the (Ti, Mo)C

6 precipitates, increasing both the precipitate volume percent and average size. Mo alloying did

7 not retard precipitation coarsening, but improved lattice misfit between precipitate and matrix,

8 contributing to better aging resistance of the Ti-Mo-alloyed steel. This new understanding

9 opens opportunities for designing aging-resistant micro-alloyed steels with lean alloying

10 elements.

11

12

13

14

15

16

17

18

19 Keywords: Micro-alloyed steel, Interphase Precipitation, Small-Angle-Scattering.

20

21

22

1 High-strength low-alloy steels strengthened through the interphase precipitation (IPP)

2 mechanism have seen a revival for automotive industry since the development of the

3 NANOHITEN steel which has tensile strengthen up to 780 MPa [1]. IPP is the phenomenon

4 that occurs upon the decomposition of austenite in steels containing strong carbide -forming

5 elements (such as Ti, Mo and V) and results in characteristic periodic planes of fine precipitates

6 [2, 3]. In low-carbon steel fine MC (M = Ti, Mo or V) IPP are encapsulated within a soft ferritic

7 matrix which is strengthened through the Orowan mechanism [4] yielding a steel with high

8 strength and formability [5].

9

10 However, these MC particles can coarsen during hot rolling or subsequent annealing heat

11 treatment, degrading the strength of the materials significantly. One possible solution reported

12 in the literature is the addition of molybdenum (Mo). Funakawa and Seto [6], and later work

13 conducted by others [7-10] found that steels with Mo additions showed that the mechanical

14 properties were retained longer during high-temperature ageing. These studies were compared

15 to the observed interphase precipitation in Ti-containing (~0.2wt%) and Ti-Mo-containing

16 (~0.1wt%Ti and ~0.2wt%Mo) low carbon steels with a fixed basic composition ~0.04%C,

17 1.5%Mn, 0.2%Si in wt.%. It can be seen that in these studies, the atomic ratio of Ti:C and

18 (Ti+Mo):C were designed to be ~1:1. The most well-known mechanism for this effect was

19 reported by Jang et al. [8], who used first principles calculations to propose that the Mo only

20 participates during the early stages of precipitation and becomes passive due to the energetic

21 disadvantage during the subsequent growth and coarsening stages. The coarsening of

22 precipitates is mainly controlled by diffusion of Ti atoms, therefore, the replacement of Ti by

23 Mo reduces the Ti concentration in the ferrite matrix, which decelerates the coarsening of (Ti,

24 Mo)C precipitates [6, 8]. Moreover, Funakawa *et al.* [6] observed that a decrease in Ti

25 concentration from 0.2wt% to ~0.1wt% without Mo additions in Ti-containing steel results in

1   similar hardness of Ti-Mo-containing one (~0.1wt%Ti and ~0.2wt%Mo). Jang *et al.*, [11] used

2   CALPHAD and diffusion simulations to show that the coarsening rate of TiC in Fe-Ti-C steels

3   (fixed 0.04%C, wt%) can be significantly retarded by decreasing the Ti/C ratio.

4

5   However, both the effect of Ti/C ratio and the Mo on the interphase precipitation have not been

6   well examined quantitatively, which leaves a question to the automotive industry whether it is

7   necessary to add Mo into Ti-containing steels. This is due to the widely used techniques such

8   as transmission electron microscopy (TEM) [12, 13] and atom probe tomography (APT) [14-

9   18] which have a limited capability to analyse statistically significant numbers of precipitates.

10   The size difference of precipiates in Ti and Ti-Mo steels presented in the literature is so small

11   (typically in the range of 1.6 nm to 10 nm [7-9]) that it is difficult to statistically and accurately

12   investigate the the role of Mo with TEM and APT.

13

14   The present study utilizes Small-Angle-Neutron-Scattering (SANS) to study the precipitation

15   behaviour of two micro-alloyed steels aged at 650°C for various times. One steel (Fe-0.079Ti-

16   0.051C-1.63Mn-0.19Si-0.036Al-0,014P-0.006S-0.007N, wt%) contains Ti with a Ti:C atomic

17   ratio of 0.4. The second steel (Fe-0.07Ti-0.2Mo-0.044C-1.58Mn-0.19Si-0.039Al-0,013P-

18   0.005S-0.0046N, wt%) contains Ti and Mo with a (Ti+Mo):C atomic ratio of ~1. The detailed

19   characterization was undertaken using SANS, through analysis of both the nuclear and

20   magnetic signals, giving quantitative insight into the evolution of the average precipitate size,

21   volume percent, and precipitate chemistry in bulk samples, which are key information to

22   uncover the precipitation kinetics and hardening behaviour. The data obtained is averaged over

23   billions of precipitates and provides new insights not available from TEM or APT where only

24   tens to hundreds of precipitates are typically measured.

1   The alloys were vacuum induction melted, casted and then forged at about 1250 °C followed

2   by air cooling. Pieces 30×10×5 mm^3 were sectioned and heat treated (See Supplementary Fig.

3   S1a). Firstly, the specimens were austenitized in a salt bath at 1250 °C for 300 s to dissolve

4   pre-existing precipitates and water quenched. Secondly, the specimens were austenitized at 950

5   °C for 120 s (to control the austenite grain size) then transferred directly to a salt bath at 650

6   °C for periods ranging from 0 to 36 ks and water quenched. Prolonged long-term ageing for a

7   further 144 ks was performed separately. The austenitization temperature of 950°C and

8   duration of 120 s were selected in order to balance the compromise between the austenite grain

9   size, the minimisation of carbide precipitation in austenite. Interphase precipitates can only

10   form at the advancing austenite/ferrite boundary an therefore, the majority of the Ti, Mo and C

11   must have remained in solution during austenization. The precipitation-time temperature

12   diagram obtained by Wang et al. [10] shows that the start times of carbide precipitation in Ti-

13   Mo (0.1%Ti-0.2Mo%) micro-alloyed steel exceeds 150 s at 950°C.

14

15   SANS experiments were performed on the SANS2d beamline at the ISIS Pulsed Neutron

16   Source, UK [19]. A magnetic field of 1.5 T was applied to saturate the ferritic matrix which

17   allows the separation of the magnetic and nuclear scattering. Specimens with dimension of ~9

18   mm×~9 mm× ~1 mm were cut from the heat treated samples for the SANS measurements. The

19   neutron beam size was 8mm in diameter and the measurement time was set to 60min. The

20   sample to detector distance was 4m which gave scattering vector, q, covered the range of 0.004

21   to 0.3 Å^{-1}. To avoid collecting scattering signal from multi-Bragg diffraction, only neutrons

22   with wavelengths, λ, from 4.5 to 16.5 Å were selected for data analysis [20]. One-dimensional

23   nuclear and "nuclear + magnetic" scattering intensity plots, I (intensity) versus q were obtained

24   by partial azimuthal averaging in 30 sectors around the horizontal and vertical axes of the

25   transmitted beam respectively using the software Mantidplot [21].

1   The microstructures of polished and 2% Nital etched samples were examined using scanning

2   electron microscopy (SEM) via an FEI Quanta 650 FEG-SEM operated at a voltage of 20 kV.

3   Detailed microstructures of the (Ti,Mo)C precipitates were examined using a JEOL 2100 TEM.

4   Thin foil specimens were mechanically polished to ~30 μm in thickness followed by ion beam

5   milling to electron transparency. The microhardness (Hv) of ferrite grains in heat treated

6   samples was measured using a microhardness tester with a load of 0.1 kgf. 20 measurements

7   were conducted for each sample.

8

9   Fig.1a shows the mean value of Hv versus age time at 650 °C for both Ti and Ti-Mo containing

10   steels and the error-bar represents one standard deviation. The Ti-Mo containing steels show

11   slightly higher hardness and better ageing-resistance compared to the steel with only Ti

12   additions. As shown in Figs. 1b and 1c, the γ to α transformation in both steels occurs rapidly

13   and both reached ~90% completion in a similar duration of 60 s. This agrees with the

14   dilatometry results (Supplementary Fig. S1b). Figs. 1b, 1c, 1d and 1e also show that

15   decreasingly small regions of bainite formed during quenching with increasing isothermal

16   holding. Both SEM and dilatometry measurements reveal that Mo has a small effect on the γ

17   to α transformation. Bright field TEM images of the Ti and Ti-Mo containing samples

18   transformed at 650°C for 36 ks are shown in Figs. 2(e) and (f). In both alloys, characteristic

19   periodic planes of nanoscale precipitates are observed, indicative of interphase precipitation.

20

21   Fig. 2 shows the one dimensional nuclear and magnetic SANS data in the form of Iq^2 versus

22   scattering vector (q) (left hand axis) for the selected isothermally transformed (60 s, 36 ks and

23   180 ks) alloys. The results for the water quenched sample and the remaining isothermally

24   transformed (0.3ks, 3.6 ks and 18 ks) samples are shown in Supplementary Figs. S2 and S3.

25   The ratio of magnetic scattering ($I_{mag}(q)$) to nuclear scattering ($I_{nuc}(q)$) intensity, $R(q)$,

1   which is related to the precipitate composition, is shown on the left-hand axis. If all precipitates

2   have the same composition then the value of $R(q)$ would be constant. On the other hand, $R(q)$

3   would vary if either there were more than one type of precipitate present of differing size or

4   the precipitate composition is size dependent [22]. Cleary, there were two types of particles

5   with significant difference in both size and composition formed in both steels revealed by two

6   different $R(q)$ values of ~3 and ~1 at low (0.004 to ~0.01 Å^{-1}) and high (0.02 to ~0.1 Å^{-1}) q

7   region respectively. A low number density of large (> 500 nm), cube-shaped TiN precipitates

8   can be formed during casting process and could remain undissolved during the experimental

9   solution treatment [10]. These large TiN precipitates only contribute to the Porod scattering at

10   low q region < 0.001 Å^{-1} and has negligible influence on the scattering signal at q region > 0.01

11   Å^{-1}.

12

13   In the low q region, $R(q)$ increases due to the presence of large iron carbides and this is seen

14   to exist in the Ti-containing steels up to 180 ks. In the Ti-Mo containing steels, there is less

15   evidence for an increase in $R(q)$ at low q suggesting less iron carbide forms in this steel. The

16   scattering from large scale iron carbides also reveals itself in the form of a Porod Law slope of

17   approximately q^{-2} on the plot of Iq^2 versus q at the low q region. These large iron carbides

18   (Figs. 1b and 1c), make only a small contribution to the nuclear scattering signal (because of

19   their small contrast factor) but a significant contribution to the magnetic scattering signal. This

20   causes to a marked difference between these two signals at low q as revealed by an increase in

21   the $R(q)$ value. In the samples isothermally held for 180 ks, the matrix phase transformation

22   was completed so iron carbides did not form following quenching resulting in a smaller

23   difference between the nuclear and magnetic signals across the entire range of q. At high q

24   region, it is the fine IPP that contribute to the nuclear and magnetic signals and so $R(q)$

25   plateaus from which the chemical composition of the IPP can be estimated. A low number

1   density of large (> 500 nm), cube-shaped TiN precipitates can be formed during casting process

2   and could remain undissolved during the experimental solution treatment [1]. These large TiN

3   precipitates only contribute to the Porod scattering at low q region < 0.001 Å^{-1} and has

4   negligible influence on the scattering signal at q region > 0.01 Å^{-1}.

5

6   To isolate the scattering signal only from nano-sized TiC or (Ti, Mo)C precipitates the Porod

7   Law region at low q and the incoherent background in both the nuclear and magnetic SANS

8   signals were subtracted. Fig. 3 shows the mean values of $R(q)$, which were calculated by taking

9   the average of $R(q)$ values in the q range from ~0.0194 to ~0.0775 Å^{-1} (for samples aged for

10   60s to 3.6 ks) and ~0.0097 to ~0.0664 Å^{-1} (for samples aged from 18 ks to 180 ks). The error

11   in Fig. 3 is given as one standard deviation. The results show that the mean values of $R(q)$ for

12   isothermally transformed Ti and Ti-Mo alloys were ~0.70 and ~0.95 respectively. The ageing

13   time did not change the mean values of $R(q)$ significantly. The theoretical $R(q)$ values of

14   ~0.64 and ~1 represent the average chemical composition of the precipitates in Ti and Ti-Mo

15   containing steels are TiC and $Ti_{0.75}Mo_{0.25}C$ respectively [21], as shown by the red and blue

16   horizontal lines in Fig. 3. The substitution of Ti with Mo in the precipitates is in excellent

17   agreement with results obtained from APT [18, 23-24] and extraction [25] in similar micro-

18   alloyed steels (e.g. 0.05% to 0.2% Ti-0.20%Mo-0.045% C, wt%).

19

20   The volume percent (f_v) of TiC and (Ti, Mo)C were calculated from the invariant, Q, of the

21   magnetic SANS signal using the equation $Q = \int_0^\infty I(q)q^2 dq = 2\pi^2 \left(\rho_\rho - \rho_m\right)^2 f_v(1-f_v)$ [21, 26].

22   where ρ_p and ρ_m are the magnetic scattering length densities of precipitate and matrix. The use

23   of magnetic SANS signal ensures that the volume percent calculation is independent of the

24   chemical composition of the precipitates. Fig. 4a shows that the volume percent of TiC in Ti

25   steels and (Ti, Mo)C in TiMo steels were ~0.10% and ~0.13% respectively and invariant with

1   isothermal holding. The equilibrium volume percent of 0.156 vol% (TiC phase fraction) and

2   0.157 vol% ((Ti, Mo)C phase fraction) at 650 °C calculated using Thermo-Calc and the TCFE7

3   database. In the Ti-Mo steel, the equilibrium atomic ratio of Ti to Mo in (Ti, Mo)C precipitates

4   is predicted to be ~9:1, which indicates the Mo is not strong stabiliser for MC-type carbide.

5

6   Figs. 4b, 4c and 4d show the Kratky radius (R_{max}), Guinier radius (R) and thickness (T) (disk

7   morphology [24]) of particles obtained from both nuclear and magnetic SANS scattering signs.

8   The Kratky radius is calculated by $R_{max} = \sqrt{3}/q_{max}$ (the "pseudo-Guinier radius"), where the

9   q_{max} determined from the the Kratky plot (Iq^2 vs q) [27]. Alternatively, a radius of gyration,

10   R_{g1}, is extracted from the Guinier plot (which takes the form of ln(I) *vs* q^2) using a self-

11   consistent method with 1<qR_{g1}<2. Considering a distribution of monodisperse thin discs of

12   thickness, T, and radius, R, the relationship between T, R and R_{g1} is given by $R^2_{g1}=T^2/12+R^2/2$

13   [28]. A second Guinier plot of $ln[q^2(I)]$ vs q^2 is known to give a radius of gyration, R_{g2}, that is

14   related to the disc thickness, $R_{g2}=(T^2/12)^{0.5}$. Fig. 4b shows that the average size of the TiC and

15   (Ti, Mo)C interphase precipitates increased from ~6.5nm after 60s to ~10nm after 3.6ks, but

16   exhibit minimal growth during the further ageing up to 180ks at 650°C. The average Guiner

17   radius (Fig. 4c) of disk precipitates has been found ~2nm smaller than Kratky radius, but

18   followed very similar tendency as kratkey radius. Fig. 4d indicated that the average Gunier

19   thicknesses of TiC and (Ti,Mo)C were ~5.5nm and ~6.5nm respectively and both exhibit

20   insignificant evolution (<1.5nm) during isothermal ageing. Hence, the hypothesis that the Mo

21   can retard the growth and coarsening of (Ti,Mo)C interphase precipitation is not supported by

22   our results, which show the average precipitate size in aged Ti-containing steels were even

23   slightly smaller than in aged Ti-Mo-containing steels.

24

25   The precipitates coarsening rates in both alloys were extremely low. In Ti-containing steels it

1   is known that a low Ti/C ratio (0.4) causes the concentration of Ti at the precipitate-ferrite

2   interface to become small and therefore the diffusion gradients which drive coarsening become

3   shallow and slow [11]. While in Ti-Mo added steels, although the Ti+Mo/C=1 and Mo

4   incorporated into the precipitates at nucleation, the subsequent growth of precipitates is

5   controlled by the diffusion of Ti atoms rather than Mo. We can conclude that the addition of

6   Mo slightly improved the ageing-resistance of the steels (Fig. 1a) is due to (Ti,Mo)C having a

7   reduced misfit strain between the carbide and ferrite matrix than TiC [8, 29], rather than Mo

8   retarding coarsening of the precipitates. Seol et al. [30] and Wang et al. [31-32] indicated that

9   Mo can segregate at precipitate's outer to form a core-shell structure with Ti-rich core and Mo-

10   rich shell. Mo layer inhibiting the diffusion of Ti, and V from the matrix into the precipitates,

11   which impedes particle coarsening. Whether this mechanism exists in Ti-Mo added steels needs

12   future investigation. The current work only shows the Mo did not retard the global growth and

13   coarsening of (Ti,Mo)C in 0.07%Ti-0.2%Mo (wt%) micro-alloyed steels.

14

15   The addition of Mo also slightly increased the hardness of the steels (Fig. 1a). This is due to

16   the higher volume percent of interphase precipitates rather than a decreased average size of

17   precipitate. Approximately 25 at.% Mo co-precipitates as (Mo,Ti)C at the early stage of

18   precipitation and this increased the volume percent of these precipitates from ~0.1% to ~0.13%.

19   This yields ~7% improvement in the precipitation strengthening effect based on the Ashby-

20   Orowan equation $\Delta\sigma_{ppt} = \frac{0.538Gbf_v^{0.5}}{2R} ln\left(\frac{R}{b}\right)$ [9, 33, 34]. Where, $\Delta\sigma_{ppt}$ is the increase in yield

21   strength, G is the shear modulus, b is the Burgers vector, f_v is the carbide volume fraction and

22   R is the mean carbide radius.

23

24   In summary, our SANS results (nuclear and magnetic scattering signals) reveal Mo does not

25   play a role in retarding nano-precipitate coarsening, which is in contrary to existing literature.

Instead, our results show that approximately 25 at.% Mo replaced Ti in the (Mo,Ti)C precipitates, increasing both the precipitate volume percent and average size, and changing the lattice spacing, altering the coherency. Ti-Mo-alloyed steel has higher volume fraction of nano-precipitates than Ti-alloyed steel hence higher hardness. The better ageing-resistance of the Ti-Mo steels than Ti only steels is mainly due to the decrease in misfit between the carbide and matrix leading to coherency being maintained at longer aging times in Ti-Mo alloyed steel. This new understanding opens opportunities for design of ageing-resistant micro-alloyed steels with significantly less amount of Mo.

References

[1] Y. Funakawa, T. Shiozaki, K. Tomita, T. Yamamoto, E. Maeda, ISIJ Int. 44(11) (2004) 1945-1951.
[2] A. Davenport, F. Berry, R. Honeycombe, Metal Sci. 2(1) (1968) 104-106.
[3] S.-P. Tsai, Y.-T. Tsai, Y.-W. Chen, J.-R. Yang, C.-Y. Chen, Y.-T. Wang, C.-Y. Huang, Scr. Mater. 143 (2018) 103-107.
[4] T. Gladman, Maney Pub1997.
[5] F. Yoshimsa, F. Takeshi, Y. Katsumi, JFE Tech. Rep. No. 18 (2013).
[6] Y. Funakawa, K. Seto, Tetsu-to-Hagane. 93(1) (2007) 49-56.
[7] C. Chen, H. Yen, F. Kao, W. Li, C. Huang, J. Yang, S. Wang, Mater. Sci. Eng. A. 499(1) (2009) 162-166.
[8] J.H. Jang, C.-H. Lee, Y.-U. Heo, D.-W. Suh, Acta Mater. 60(1) (2012) 208-217.
[9] N. Kamikawa, Y. Abe, G. Miyamoto, Y. Funakawa, T. Furuhara, ISIJ Int. 54(1) (2014) 212-221.
[10] Z. Wang, H. Zhang, C. Guo, W. Liu, Z. Yang, X. Sun, Z. Zhang, F. Jiang, J. Mater. Sci. 51(10) (2016) 4996-5007.

[11] J. Jang, C. Lee, H. Han, H. Bhadeshia, D. Suh, Mater. Sci. Technol. 29(9) (2013) 1074-1079.

[12] H.-W. Yen, P.-Y. Chen, C.-Y. Huang, J.-R. Yang, Acta Mater. 59(16) (2011) 6264-6274.

[13] H.-W. Yen, C.-Y. Huang, J.-R. Yang, Scripta Mater. 61(6) (2009) 616-619.

[14] Y.-J. Zhang, G. Miyamoto, K. Shinbo, T. Furuhara, Scr. Mater 69(1) (2013) 17-20.

[15] Y. Kobayashi, J. Takahashi, K. Kawakami, Scr. Mater. 67(10) (2012) 854-857.

[16] I. Timokhina, P. Hodgson, S. Ringer, R. Zheng, E. Pereloma, Scr. Mater. 56(7) (2007) 601-604.

[17] C. Enloe, K. Findley, C.M. Parish, M.K. Miller, B. De Cooman, J. Speer, Scr. Mater. 68(1) (2013) 55-58.

[18] J. Wang, M. Weyland, I. Bikmukhametov, M.K. Miller, P. D. Hodgson, I. Timokhina, Scr. Mater. 160 (2019) 53-57.

[19] R. Heenan, S. Rogers, D. Turner, A. Terry, J. Treadgold, S. King, Neutron News 22(2) (2011) 19-21.

[20] A. Michels, J. Weissmüller, Rep. Prog. Phys 71(6) (2008) 066501.

[21] Y. Wang, S. Clark, V. Janik, R. Heenan, D.A. Venero, K. Yan, D. McCartney, S. Sridhar, P. Lee, Acta Mater. 145 (2018) 84-96.

[22] B.S. Seong, E. Shin, S.-H. Choi, Y. Choi, Y.S. Han, K.H. Lee, Y. Tomota, Appl. Phys. A 99(3) (2010) 613-620.

[23] I. Bikmukhametov, H. Beladi, J. Wang, P. D. Hodgson, and I. Timokhina, Acta Mater. 170 (2019) 75-86.

[24] S. Mukherjee, I. Timokhina, C. Zhu, S. Ringer, P. Hodgson, Acta mater. 61(7) (2013) 2521-2530.

[25] Y. Tanaka, S. Kinoshiro, H. Nakamichi, JFE Tech. Rep. No. 37 (2016) 31-36.

[26] F. De Geuser, A. Deschamps, C R Phys 13(3) (2012) 246-256.

[27] A. Deschamps, F. De Geuser, J. Appl. Crystallogr. 44(2) (2011) 343-352.

[28] H. Yasuhara, K. Sato, Y. Toji, M. Ohnuma, J. SUZUKI, Y. Tomota, Tetsu-to-Hagane. 96(9) (2010) 545-549.

[29] J. Jang, Y. Heo, C. Lee, H. Bhadeshia, D.-W. Suh, Mater. Sci. Technol. 29(3) (2013) 309-313.

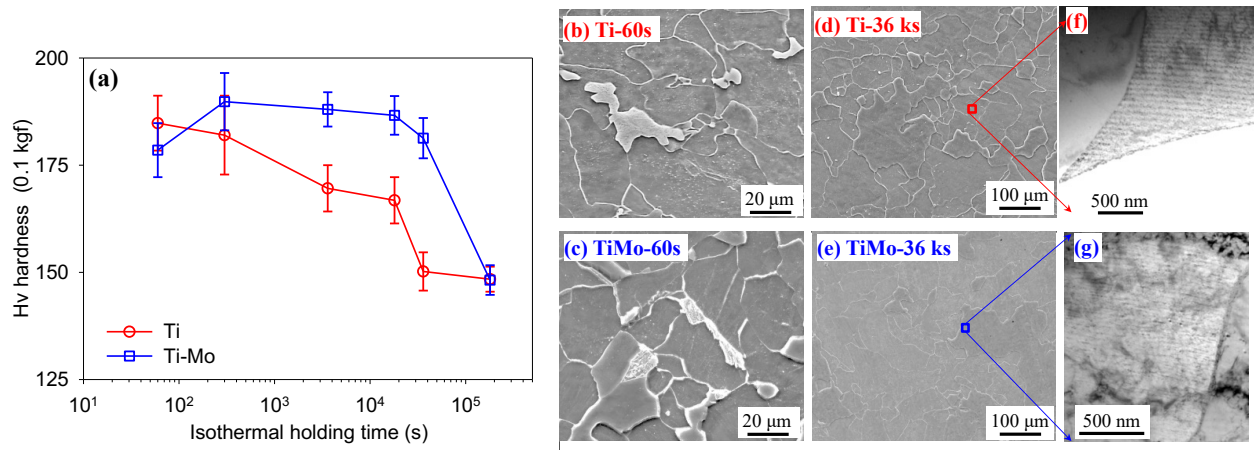[30] Z. Wang, H. Chen, Z. Yang, F. Jiang, Metall. Mater. Trans. A 49, no. 5 (2018): 1455-1459.

[31] Z. Wang, X. Sun, Z. Yang, Q. Yong, C. Zhang, Z. Li, Y. Weng, Mater. Sci. Eng. A. 573 (2013): 84-91.

[32] J. B. Seol, S. H. Na, B. Gault, J. E. Kim, J. C. Han, C. G. Park, D. Rabbe, Sci. Rep. 7 (2017) 42547.

[33] M.-Y. Chen, M. Gouné, M. Verdier, Y. Bréchet, J.-R. Yang, Acta Mater. 64 (2014) 78-92.

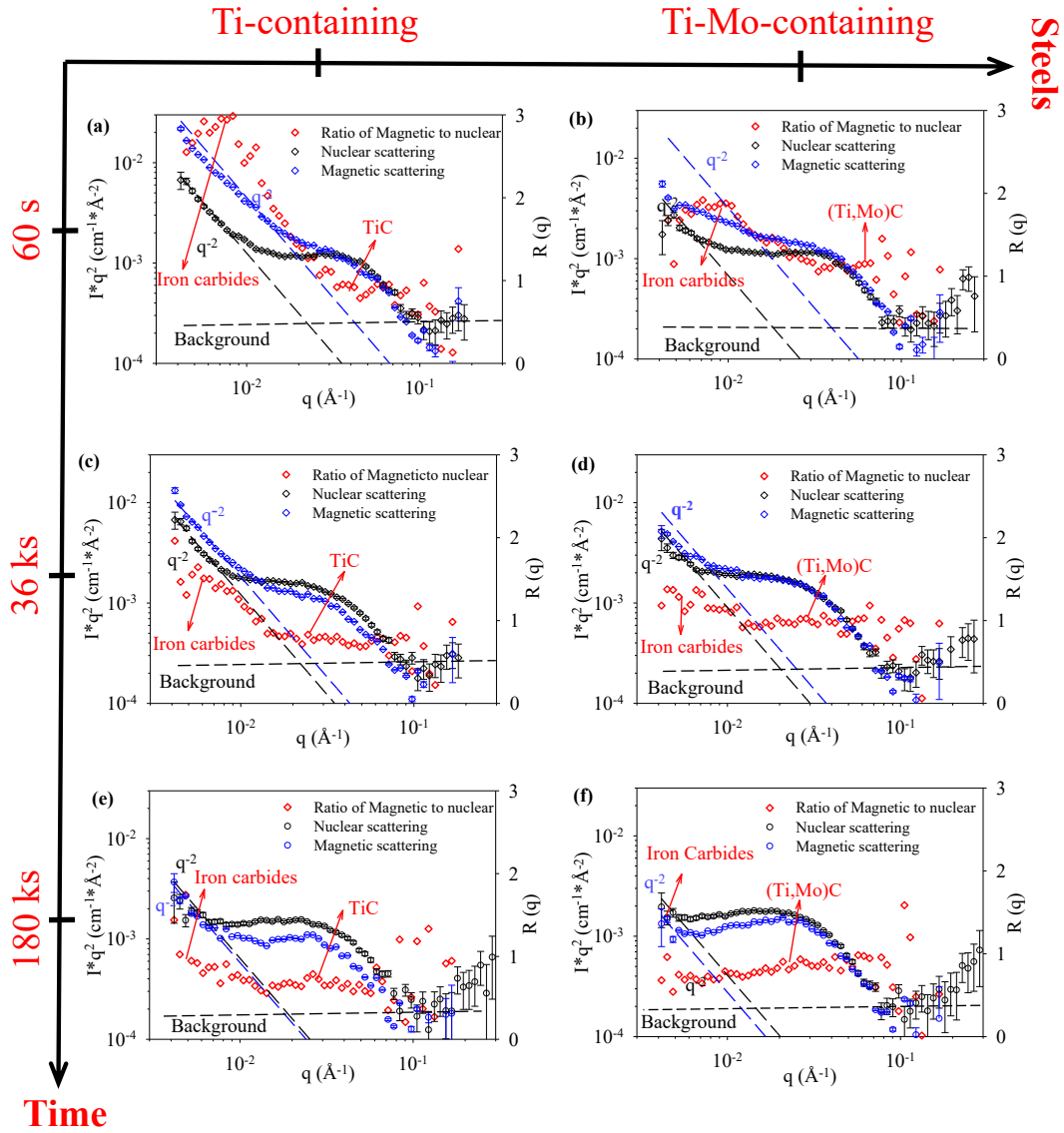[34] P. Gong, X. Liu, A. Rijkenberg, W. Rainforth, Acta Mater. 161 (2018) 374-387.

Fig. 1. (a) Effect of isothermal holding time, t, on measured microhardness, Hv, of the Ti and Ti-Mo steels held at 650 °C. Error bars in Hv correspond to one standard deviation from the mean. (b) to (e) SEM images of the Ti (b and c) and TiMo (d and e) samples isothermally transformed for 60 s and 36 ks. (f) and (g) Bright field TEM images of the Ti and TiMo steels respectively after ageing for 36 ks showing interphase precipitation.
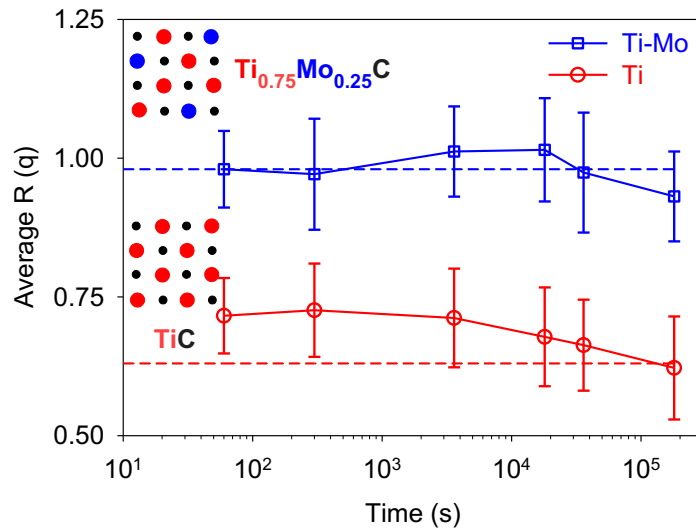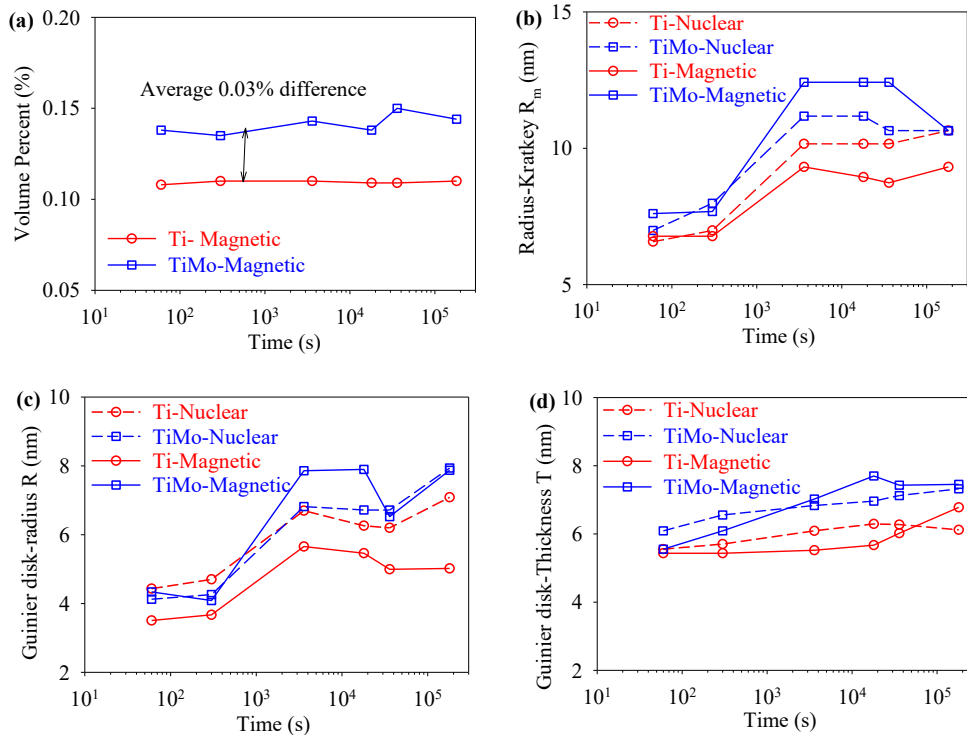
Fig. 2. One-dimensional nuclear and magnetic SANS patterns of Iq^2 (left hand axis) and $R(q)$ (right hand) axis versus scattering vector, q, obtained from the (a, c and e) Ti and (b, d, and f) TiMo samples isothermally transformed at 650 °C for (a and b) 60 s, (c and f) 36 ks, (e and f) 180 ks respectively.

14

1

Fig. 3. Plot of the mean value of R(q) as a function of scattering vector, q, calculated from the scattering curves in Fig. 2. R(q) is the ratio of magnetic to nuclear scattering intensity. Theoretical values for TiC and for $Ti_{0.75}Mo_{0.25}C$ are shown by the horizontal lines.

Fig. 4. Graphs to show the effect of isothermal holding time, t on carbide particle volume fraction and particle dimensions in Ti and TiMo alloys aged at 650 °C. (a) Particle volume percent calculated from analysis of the invariant, Q, of the magnetic SANS data. Particle dimensions obtained from (b) Kratky radius, R_{max}, assuming spherical-shaped particles and (c and d) Guinier analysis assuming disk-shaped particles. (c) shows the disk radius, R, versus ageing time, t, and (d) shows disk thickness, T, versus time, t.

15